

## Article

# The Evaluation of Rock Mass Characteristics against Seepage for Sustainable Infrastructure Development

Muhammad Nasir Khurshid <sup>1,\*</sup>, Ammad Hassan Khan <sup>1</sup>, Zia ur Rehman <sup>1</sup> and Tahir Sultan Chaudhary <sup>2</sup>

<sup>1</sup> Department of Transportation Engineering and Management (DTEM), University of Engineering and Technology (UET), G.T. Road, Lahore 54890, Pakistan

<sup>2</sup> Department of Civil Engineering, Bahauddin Zakariya University (BZU), Multan 60800, Pakistan

\* Correspondence: 2019phdte03@student.uet.edu.pk

**Abstract:** The determination of rock seepage characteristics is a complex phenomenon due to the variability, discontinuities, and formation age of rocks. The available literature on rock mechanics covers empirical relationships and approaches for the estimation of seepage characteristics from the rock mass parameters. In this study, an area comprising of infrastructure such as a water reservoir, embankments, roads, etc., constructed on mix rock mass formations was selected. The field and laboratory tests' geo-mechanical data for the study area were evaluated. The data obtained from the field geo-mechanical engineering tests like Rock Quality Designation (RQD), Rock Core Recovery, Lugeon, etc., were analyzed. The data retrieved from the geological and geotechnical laboratory tests such as petrography, uniaxial compression, Hoek shear, elastic modulus, etc., were also evaluated. Rock mass was characterized based on petrographic and RQD, and was found in the hybrid formation of igneous, metamorphic, and sedimentary deposits. Seepage analysis in the study area was also carried out based on adit and piezometric data (installed in accordance with the mining technology guidelines), using Seep W Finite Element Method (FEM). The seepage observed in adits were compared with seepage calculated from Seep W. The trend of simulated flux was also presented against K ratio. Seepage quantities for different ranges of K ratio were plotted to evaluate interdependency between seepage and K ratio. Correlations of RQD were developed with hydraulic conductivity "k" for igneous, metamorphic, and sedimentary rocks for quick assessment of seepage characteristics of rock mass by RQD. These correlations and seepage related evaluations will be beneficial for the characterization of rock mass in relation to seepage for sustainable infrastructure development.

**Keywords:** rock mass; hydraulic conductivity; sustainability; rock mechanics; geotechnical engineering; geomechanical engineering; mining technology



**Citation:** Khurshid, M.N.; Khan, A.H.; Rehman, Z.u.; Chaudhary, T.S. The Evaluation of Rock Mass Characteristics against Seepage for Sustainable Infrastructure Development. *Sustainability* **2022**, *14*, 10109. <https://doi.org/10.3390/su141610109>

Academic Editors: Mahdi Hasanipanah, Danial Jahed Armaghani, Jian Zhou and Kaihui Li

Received: 28 April 2022

Accepted: 10 August 2022

Published: 15 August 2022

**Publisher's Note:** MDPI stays neutral with regard to jurisdictional claims in published maps and institutional affiliations.



**Copyright:** © 2022 by the authors. Licensee MDPI, Basel, Switzerland. This article is an open access article distributed under the terms and conditions of the Creative Commons Attribution (CC BY) license (<https://creativecommons.org/licenses/by/4.0/>).

## 1. Introduction

A large percentage of the earth surface is comprised of rocks. This makes rocks one of the significant areas of study for researchers. Rock is a basic unit of rock mass. Rock mass needs to be studied for resilient development leading to a sustainable environment, as the desired carbon emission is less during infrastructure developments [1]. Various researchers performed risk assessments for large infrastructure development projects using techniques ranging from conventional to hybrid nature to make them more sustainable [2]. The isotropic and anisotropy behavior of rock was studied by various researchers. The behavior of rock is different in an anisotropy condition as compared to normal isotropic conditions [3].

Rock mass is a collection of a rock body, which has distinct rock features like discontinuities, joints, and different planes of orientation. Types of rock mass are defined based on its classification systems. There are a number of rock mass classification systems with different relevant significance and uses. A few of them are Rock Quality Designation

(RQD), Barton Q system, and Rock Mass Rating (RMR). Among these, RQD is the most widely used rock classification system.

When a rock mass is in contact with water, the water tries to migrate into the pores of the rock mass and into the fractures. This penetration of water into the openings creates reduction in effective stress. This reduction in effective stress can reduce the strength and cause sliding of the water-affected mass. This water-affected mass, when holding material above it, leads to overall sliding of the inclined rock mass, causing slope failures. The cases of rock mass failures prone to seepage have been observed in different parts of the world in recent years. The ease with which fluid may travel through rock mass is termed seepage. The rock mass that allows a higher quantity of fluid to flow through it with more ease is more seepage prone compared to one that exhibits more resistance to the flow of fluid through it. The seepage of rock mass is governed by fractures. If the discontinuities are open and wide, the ease of the flow of fluid through rock mass will increase. The seepage can be estimated through the hydraulic conductivity of rock mass. The hydraulic conductivity is more often used in rock mass to represent the seepage. For determination of rock mass hydraulic conductivity in the field, the Lugeon test, also known as Water Pressure Test (WPT), can be used [4,5]. For determination of hydraulic conductivity in the field and in the laboratory, the Darcy (1856) relation can be used, as follows:

$$Q = AV = Aki \quad (1)$$

where “Q” is the rate of flow in m<sup>3</sup>/sec, “A” is the cross-sectional area, “i” is the hydraulic gradient measured in the direction of flow, and k (m/sec) is the hydraulic conductivity.

Various researchers have determined patterns of hydraulic conductivity in rock mass fractures. They have proposed treatment methods for the rock mass fractures to make them more durable/sustainable against the effects of seepage. Hydraulic conductivity validation in rock mass fractures in mining technology has also been experimentally and numerically modeled by various researchers in the past [6–10]. Table 1 shows few noticeable correlations established between hydraulic conductivity and RQD.

**Table 1.** Summary of noticeable correlations available in literature between rock quality designation (RQD) and hydraulic conductivity.

Sr. No.	Equation	R <sup>2</sup>	Rock Type	Data Type	Reference
1	$k = 177.45 \times e^{-0.0361 \times RQD}$	0.64		Borehole data	[11]
2	$k = 890.9 \times e^{-0.0559 \times RQD}$	0.87	Sedimentary	Field mapping data	[11]
3	$k = 0.01382 - 0.0031 \ln RQD$	0.70		Borehole data	[12]

Where k is hydraulic conductivity and RQD is rock quality designation.

The rock mass internal and external factors deciding its mechanical behavior are key for its sustainable evaluation. Rock mass internal factors include pattern of discontinuities, strength/stiffness, fracture, behavior, friction factor, fracture distribution, etc. The effect of secondary constituents like clay filling and chemical changes causing variations in the rock mass discontinuities was studied by various researchers [5,13–22]. There are several external factors of rock mass such as location, geological formation, and type of infrastructure. Various infrastructures cause stress removal caused by excavation, fracture filling due to a water reservoir, fluid injection due to hydro-fracturing, and associated activities (oil and water), causing stress changes in rock fault, etc., which affect its behavior [8,10,23–28]. Literature reported the typical ranges of internal and external factors of rock mass. For evaluation of these factors, different destructive and nondestructive techniques can be employed [4,29–31]. Various simulation tools were also discussed in different studies for the prediction of rock mass internal and external factors. These simulation tools were employed to evaluate the response of external factors to interval properties of rock mass [6,7,9,32–41].

It is well established that for any infrastructure built on or in the rock mass, the seepage may affect its sustainability, including service life, working conditions, utility,

etc. [26–28,32,42]. The assessment of the hydraulic conductivity of rock mass allows the designers, constructors, and operators to forecast the response of rock mass against seepage behavior during sustainable evaluation of the infrastructure.

The effect of seepage can contribute, in a number of ways, to harming not only general ground conditions but also infrastructure facilities. Man-made activities such as blasting also affect the seepage in rock mass by causing destruction (opening of joints), affecting the steady state regime in comparison to pre-blast rock mass characteristics [25]. In addition to total failures, the problem of seepage poses threats to the stability of structures such that the cost of repairs becomes higher than original measures adopted at the time of design, as shown in Figure 1.

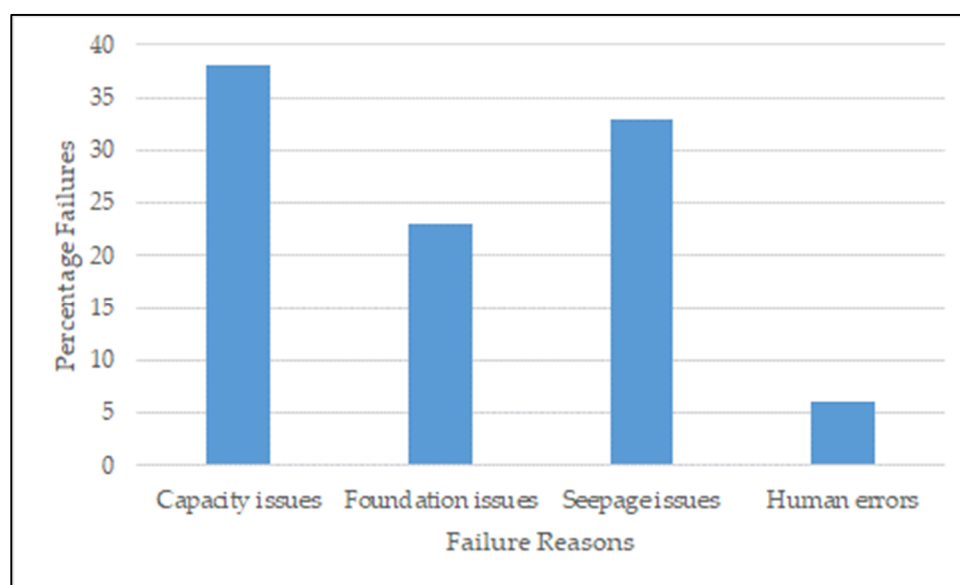


**Figure 1.** Summary of the seepage contribution in infrastructure failures constructed on rock mass.

Rock Quality Designation (RQD) is one the most quickly determinable rock mass parameters that can be evaluated with relative ease. Hence, in literature, an attempt was made by most of the researchers to correlate RQD with hydraulic conductivity. The correlations available for rock mass composite formations are quite limited in literature. This may be due to the rock mass' variations and its relatively non-homogenous behavior. The high cost of field and laboratory tests of rock mass is another significant factor.

An attempt was made in this study to identify rock mass formations surrounded by developed infrastructures and water front. Characterization of rock mass and its respective seepage response was planned to be determined from the geomechanical engineering database of the developed infrastructures by developing suitable correlations. The seepage and pressure head database from the adits and installed piezometers (in accordance with mining technologies) was also planned to be compared with actual seepage observed in the rock mass through Finite Element Model (FEM). The behavior of rock mass related to seepage was planned to be investigated by changing hydraulic conductivity, during preparation of model. The finite element methods (FEM) was used and both rock mass characteristics and hydraulic conductivity parameters, were varied in the FEM model. These variations in FEM models were carried out to observe the response of seepage due to change of rock mass characteristics. The FEM model results were validated with seepage results obtained from field instrumentations.

## 2. Materials and Methods

The following methodology was devised to achieve the objectives of the study:

- Extensive review of literature related to rock mass formation, distribution, and seepage characteristics in Pakistan and other countries. Different stakeholders involved in the infrastructure development projects on rock mass, such as the Geological Survey of Pakistan (GSP), Water and Power Development Authority of Pakistan [43], etc., were approached for guidance in study area selection and a collection of necessary geo-mechanical engineering data.
- Based on a review of literature and meetings with stakeholders, the study area was selected.
- A reconnaissance survey was carried out as per the guidelines of International Society of Rock Mechanics (ISRM) for study area profiling.
- Analysis of rock mass types, discontinuities/fault lines, etc., of the study area was carried out from the database of the Geological Survey of Pakistan.
- Field and laboratory tests (rock coring, Lugeon, uniaxial, triaxial, Hoek direct shear, point load index, etc.) and data (geological and geotechnical) obtained from WADPA were analyzed in accordance with relevant ASTM/ISRM standards.
- The rock types were classified based on the Rock Quality Designation (RQD) classification system and petrographic analysis. Determination of different rock mass properties including RQD, hydraulic conductivity, uniaxial compression strength, cohesion, friction angle, tensile strength, young's modulus, poisson's ratio, specific gravity, void ratio, water absorption, seepage characteristics (hydraulic conductivity (K), anisotropy hydraulic conductivity (K ratio ( $K_y/K_x$ )), etc., were carried out.
- A seepage analysis model of the rock mass observed at the study area was also prepared using Seep W software. The input parameters, such as K,  $K_y/K_x$ , and boundary conditions were established for the model, keeping the nomenclature of the study area.
- In the study area, actual seepage data obtained from adits and piezometers were also compared with seepage characteristics (discharge and pressure head) obtained through Finite Element Model (FEM) Seep W model. Trends between seepage characteristics in rock mass were also plotted for assessment of the necessary seepage profile of the rock mass.
- Suitable correlations between RQD and hydraulic conductivity for observed rock mass were proposed.

The characterization of identified rock mass deposits in the study area and evaluation of their seepage behavior for utilization in possible future infrastructure developments of similar rock mass types was the most important objective of this study.

### 3. Results & Discussions

Various literature sources such as journals, books, conference proceedings, reports, etc., related to the topic under study were consulted. Nomenclature of rock mass formation was evaluated in detail. The information obtained from literature was discussed with the experts from the WAPDA and GSP. The stakeholders were briefed about the objectives of the study area selection; that the area should comprise rock mass formation along with existing infrastructures close to the waterfront.

The Himalayan mountain-system of South-Central Asia in the northwestern part of Pakistan was selected as the study area (Figure 2). The region is primarily comprised of composite rock mass types, i.e., igneous, sedimentary, and metamorphic. The geological distribution primarily observed was non-fossiliferous deposits and gabbroic (dolerite/diabase) intrusions (Precambrian to Permian age). The reconnaissance survey results also revealed that the rock mass formations were developed due to tectonic and extensive folding of the geological structure. The shearing and faulting patterns can be associated with Indian sub-continental crustal deformation that arose under thrust in the Indian sub-continental plate below the Eurasian plate.



**Figure 2.** Location plan of study area.

ISRM recommended to carry out rock mass profiling using visual inspection and photographic techniques. The same guidelines were adopted in this study. After selection of the study area, detailed site visits were carried out for necessary profiling of the study area through visual inspection, meetings with local stakeholders, and photographic records.

Figure 3 shows the distribution of existing infrastructures such as roads, embankments, waterfront, rock mass, etc., at the study area.



**Figure 3.** Details of the study area during reconnaissance. (a) A view of rock mass with a road passing on the front. (b) Rock mass cut slopes facing the waterfront.

During reconnaissance, the stakeholders' representative at the study area jurisdiction were also contacted for historical database collection and seepage monitoring locations identification. Figure 4 shows location of a few of the existing instrumentation at the study area. The locations of field and laboratory tests points obtained from WAPDA database were also verified. The experiences of local stakeholders about the rock mass and its behavior in relation to the seepage was also brought on record.



**Figure 4.** Study area details observed during reconnaissance. (a) View of an adit shown in cut slopes. (b) Piezometer installed.

Figure 5 shows that the study area comprises of composite rock mass types, i.e., igneous (quartzite), metamorphic (schist), and sedimentary (limestone, shale). The igneous rock observed was intrusive in nature and without bedding planes. These rocks usually were found less seepage-prone in response. The sedimentary and metamorphic rocks were found with more discontinuities and bedding planes resulting in more seepage-prone behavior. The orientation, location, and distribution of fault lines in rock mass may impact the critical seepage path to be used during FEM analysis. The seepage values determined from field instrumentation may also show inconsistency due to presence of faults in the rock mass. The seepage response against rock mass composite formation is a quite complex phenomenon. Very often during seepage analysis in such formations, the weakest rock type is modeled as a representative of the whole formation, which may not be the representative of actual field conditions. Correlations between rock formation and quantity of seepage are also not commonly available in literature.

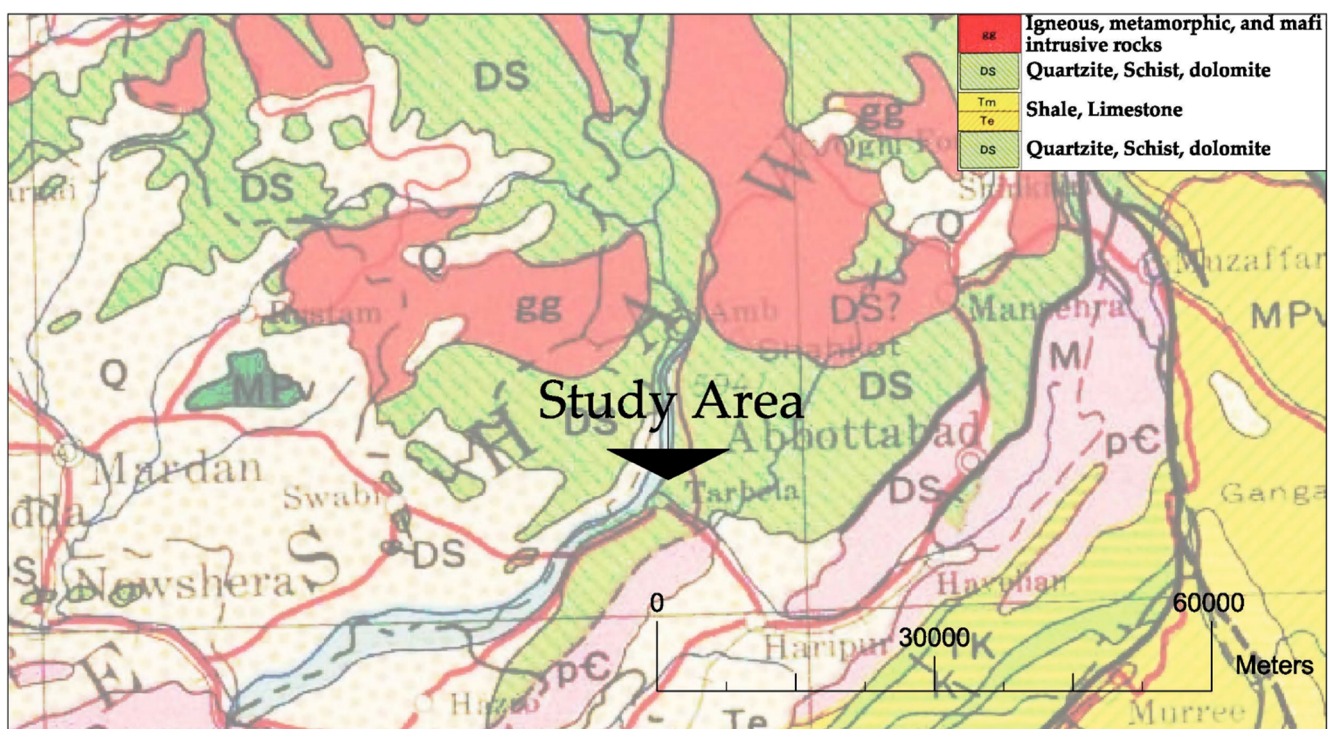


**Figure 5.** Geological map of the study area.

Details of field and laboratory explorations at the study area are summarized in Table 2, as received from WAPDA. The location of seventeen boreholes was also marked during reconnaissance, as shown in Figure 6. The data obtained from field and laboratory tests were analyzed and evaluated; the summary of which is presented afterwards. Boreholes were drilled in the rock mass formation by straight rotary drilling method using double tube core barrel of NQ/NX size. The maximum depth of a borehole was 120 m. The rock core samples were retrieved from the boreholes and preserved for laboratory testing at regular interval. Lugeon tests were performed in boreholes at regular intervals of 3 to 5 m depth. A total of 1234 RQD observations were made in the boreholes and a total of 161 Lugeon tests were performed in the boreholes. Thirteen boreholes were drilled vertically; two at an inclination of 30 degrees and two were drilled horizontally. The rock mass samples collected from each borehole were subjected to laboratory evaluation. The laboratory tests' matrix was planned in a way to record physical, strength, and elastic properties of the rock mass at different depths of borehole exploration. Some typical photographic records of the rock cores obtained from the boreholes are shown in Figure 7.

The summary of the typical range of core recovery (percentage), RQD, and Lugeon observed in different boreholes is presented in Table 3. The representative rock core samples obtained from the boreholes based on typical RQD range were subjected to petrographic analysis in the laboratory. Presented in Table 4 are the results of petrographic analysis. The results of petrographic analysis show that igneous formation with RQD 0–100 is comprised primarily of amphibole and plagioclase. Sedimentary formation with RQD 0–98 is comprised predominantly of calcite. Similarly, metamorphic formation with RQD 0–80 is comprised predominantly of quartz and muscovite/sericite. The results of RQD and petrographic analysis were used for primary and secondary rock classification, as shown in Table 3.

Figure 8 shows a typical subsurface profile of rock mass formation based on the analysis of boreholes and laboratory test data. The Natural Moisture Content (NMC) varies up to 0.4% for igneous, 3.34% for metamorphic, and 0.97% for sedimentary rocks. The unconfined compressive (UCS) strength values vary from 14 to 274 MPa for igneous, 14 to 153 MPa for metamorphic, and 43 to 105 MPa for sedimentary rocks. The UCS values observed in igneous, metamorphic, and sedimentary rock mass deposits are comparable with the UCS values reported in ISRM. The point load strength values changes from 1.84 to 15.58 MPa for igneous, 0.61 to 6.03 MPa for metamorphic, and 1.05 to 5.51 MPa for sedimentary rocks, respectively. The typical Brazilian tensile strength values range from 8.79 to 19.91 MPa for igneous, 7.58 to 11.06 MPa for metamorphic, and 7.29 to 22.02 MPa for sedimentary rock mass. The cohesion through Hoek direct shear test was found in a range of 0.01 to 0.53 MPa and 7.29 to 13.56 MPa; similarly, the friction angle from Hoek direct shear test ranges from 21.1 to 42.1 degree for igneous and 13.56 to 14.29 degree for sedimentary rocks. The values of Young's modulus vary from 17,400 to 301,000 MPa for igneous, 17,200 to 82,600 MPa for metamorphic, and 28,100 to 69,900 MPa for sedimentary rock mass. Table 5 shows the summary of typical range of geotechnical and geological engineering parameters in rock mass.

A seepage analysis model of the rock mass observed at the study area was also prepared using Seep W software. The input parameters such as K,  $K_y/K_x$ , and boundary conditions were established for the model, keeping the nomenclature of the laboratory and field test data of the study area.

To assess seepage characteristics of rock mass, a steady state seepage analysis was performed. A computer program, Seep W based on Finite Element Model (FEM), was used for analysis. The seepage analysis was carried out using a test cross section of the existing waterfront shown in Figure 9. The test cross-section was carefully prepared to include the existing instrumentation (adits and piezometers), with respect to their locations and elevations. The reservoir level at the upstream of this cross-section was at 472.5 m, while downstream it was at 341 m level.

**Table 2.** Details of geological and geotechnical exploration.

Borehole No.	Depth (m)	BH. Inclination Degree	RQD No.	Lugeon No.	Bulk Density	NMC * [44]	Water Absorption (%) [45]	Sp. Gravity [45]	UCS *** [46]	Point Load Strength [47]	Brazilian Tensile Strength [48]	Hoek Direct Shear [49]	Young's Modulus [46]	Poisson's ratio [46]
Field Testing					Laboratory Testing									
BH-01	60	Vertical	61	5	✓	✓	✓	✓	✓	✓	✓	✓	✓	✓
BH-02	100	Vertical	20	3	✓	✓	✓	✓	✓	✓	✓	✓	✓	✓
BH-03	35	Vertical	77	14	✓	✓	✓	✓	✓	✓	✓	✓	✓	✓
BH-04	35	Vertical	116	18	✓	✓	✓	✓	✓	✓	✓	✓	✓	✓
BH-05	20	Vertical	62	12	✓	✓	✓	✓	✓	✓	✓	✓	✓	✓
BH-06	110	Vertical	49	6	✓	✓	✓	✓	✓	✓	✓	✓	✓	✓
BH-07	20	Vertical	29	3	✓	✓	✓	✓	✓	✓	✓	✓	✓	✓
BH-08	90	Vertical	82	12	✓	✓	✓	✓	✓	✓	✓	✓	✓	✓
BH-09	120	30°	117	15	✓	✓	✓	✓	✓	✓	✓	✓	✓	✓
BH-10	80	Vertical	156	9	✓	✓	✓	✓	✓	✓	✓	✓	✓	✓
BH-11	50	Hor. **	44	10	✓	✓	✓	✓	✓	✓	✓	✓	✓	✓
BH-12	50	Hor. **	62	3	✓	✓	✓	✓	✓	✓	✓	✓	✓	✓
BH-13	120	Vertical	14	1	✓	✓	✓	✓	✓	✓	✓	✓	✓	✓
BH-14	100	30°	0	1	✓	✓	✓	✓	✓	✓	✓	✓	✓	✓
BH-15	115	Vertical	90	13	✓	✓	✓	✓	✓	✓	✓	✓	✓	✓
BH-16	100	Vertical	106	18	✓	✓	✓	✓	✓	✓	✓	✓	✓	✓
BH-17	100	30°	149	18	✓	✓	✓	✓	✓	✓	✓	✓	✓	✓

\* Natural Moisture Content, \*\* Horizontal, \*\*\* Uniaxial compressive strength.

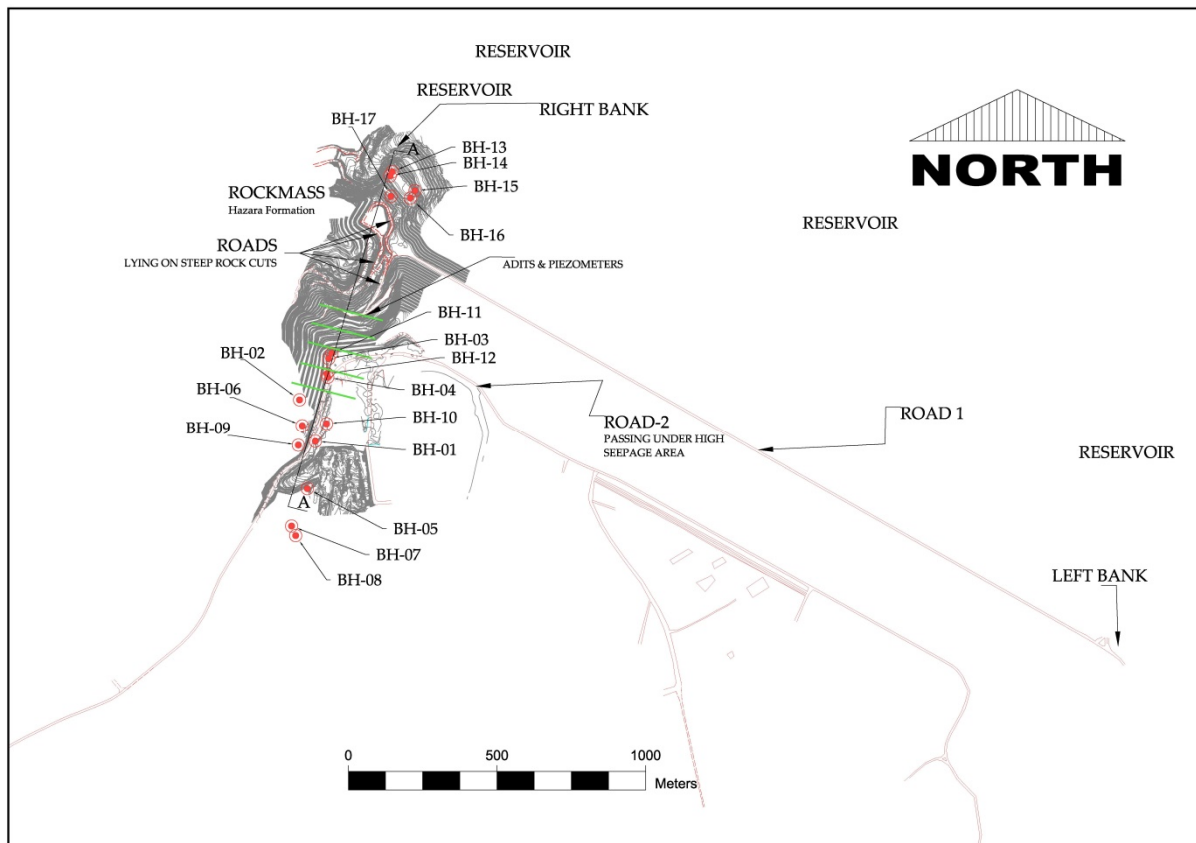


**Figure 6.** Details of the study area.

Seep W module uses the nodal mesh structure of elements, with defined material properties and boundary conditions, to evaluate the quantity of seepage through the rock mass. A 5 m mesh size was used in the model. Two-dimensional seepage flows through a rock mass in Seep W was calculated by following differential equation, which is a combination of Laplace and Darcy's law:

$$\frac{d}{dx} \left( K_x \frac{dH}{dx} \right) + \frac{d}{dy} \left( K_y \frac{dH}{dy} \right) + Q = \frac{d\theta}{dt} \quad (2)$$

where "H" is total head, "K<sub>x</sub>" and "K<sub>y</sub>" is the hydraulic conductivity in x and y direction, "Q" is the boundary flux defined, "θ" is the volumetric water content, and "t" is time.

The average values of the Lugeon test for sedimentary/metamorphic rock mass were evaluated and converted to respective hydraulic conductivity. The anisotropy property K Ratio (K<sub>y</sub>/K<sub>x</sub>) was varied in a range of 0.5 to 10 to see respective seepage and pressure head response in rock mass. The reason for K ratio variation was that the exact method to determine K ratio was not well established. The analysis was carried out keeping the rotation effect as zero, in steady state conditions with the function of pore water pressure inactive. The boundary conditions were modeled to simulate the field conditions of the study area (Figure 10). These field conditions include reservoir pressure head (water elevation) state conditions. These boundary conditions were modeled as pressure head in the form of total elevation head of water. The downstream boundary condition was kept as potential seepage face. The reason for keeping the downstream potential seepage face is to allow any flow of fluid, simulating actual field conditions. The instrumentation in the form of flow measuring adits and piezometers present at the study area was also modeled. The adits were modeled as circular region. The boundary condition for these regions for adits were defined as the elevation head, to simulate the fact that pressure will drop to the respective elevation level and any excess pressure will release in the form of seepage at

these locations. To measure the seepage quantity, flux sections were marked around these circular regions for adits. Similarly, the piezometers were modeled by adding points at the tip elevation of the mesh. These defined nodal points at the piezometer locations were used to get the results of total and pressure head.



(a)



(b)



(c)

Figure 7. Typical rock core samples observed in (a) igneous rocks, (b) metamorphic rocks, (c) sedimentary rocks.

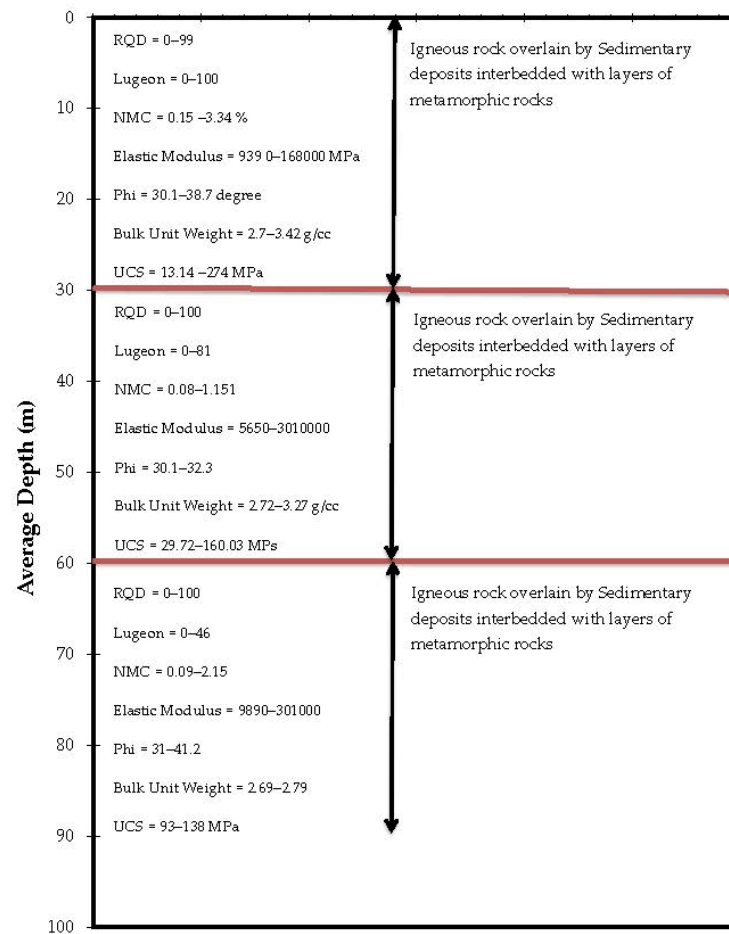
**Table 3.** Typical ranges of Core Recovery, RQD, and Lugeon values obtained in rock mass.

Bore Hole No.	Core Recovery (%)	RQD Values (%)	Lugeon Values	Primary Rock Type	Secondary Rock Type
BH-01	0–100	0–76	25–68	Metamorphic/Sedimentary	Schist/Limestone
BH-02	10–100	4–80	13–44	Metamorphic/Sedimentary	Schist/Limestone
BH-03	0–100	0–99	1–38	Metamorphic/Sedimentary	Schist/Limestone
BH-04	10–100	0–100	0.40–35	Metamorphic/Sedimentary	Schist/Limestone
BH-05	0–100	0–100	1–81	Metamorphic/Sedimentary	Schist/Limestone
BH-06	0–100	0–92	1–22	Metamorphic/Sedimentary	Schist/Limestone
BH-07	0–100	0–99	31–86	Metamorphic/Sedimentary	Schist/Limestone
BH-08	0–100	0–98	1–67	Metamorphic/Sedimentary	Schist/Limestone
BH-09	0–100	0–63	1–46	Metamorphic/Sedimentary	Schist/Limestone
BH-10	0–100	0–89	12–100	Metamorphic/Sedimentary	Schist/Limestone
BH-11	30–100	0–61.8	6–63	Metamorphic/Sedimentary	Schist/Limestone
BH-12	8–100	0–88	7–14	Metamorphic/Sedimentary	Schist/Limestone
BH-13	40–100	0–87	28–28	Igneous	Dolerite
BH-14	32–90	0–76	35–35	Igneous	Dolerite
BH-15	0–100	0–92	1–25	Igneous	Dolerite
BH-16	0–100	0–92	0.68–45	Igneous	Dolerite
BH-17	0–100	0–96	0.58–85	Igneous	Dolerite

**Table 4.** Petrographic test results.

Rock Type *	Typcial RQD %	Petrographic Results
Igneous	0–100	Amphibole 45.5%, Plagioclase 33.5%
Sedimentary	0–98	Predominantly Calcite Mineral
Metamorphic	0–80	Quartz 26.5%, Muscovite/Sericite 24%

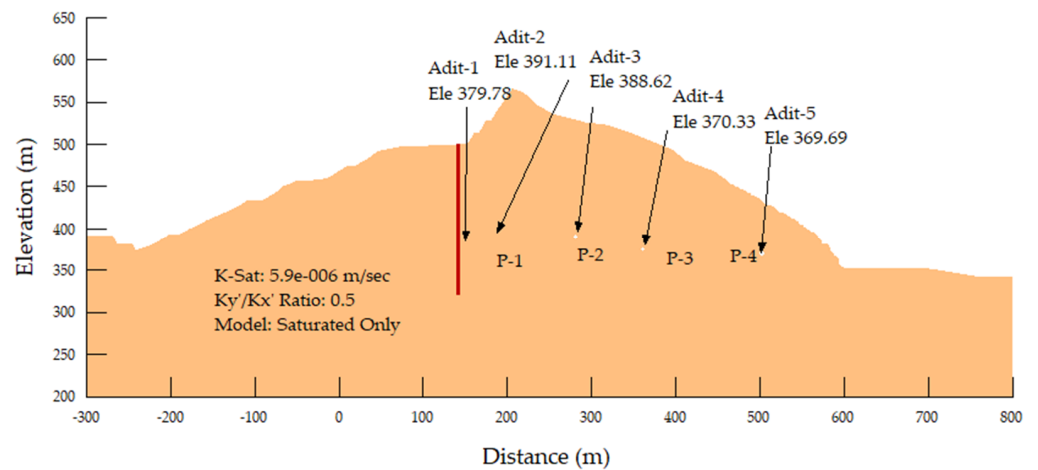
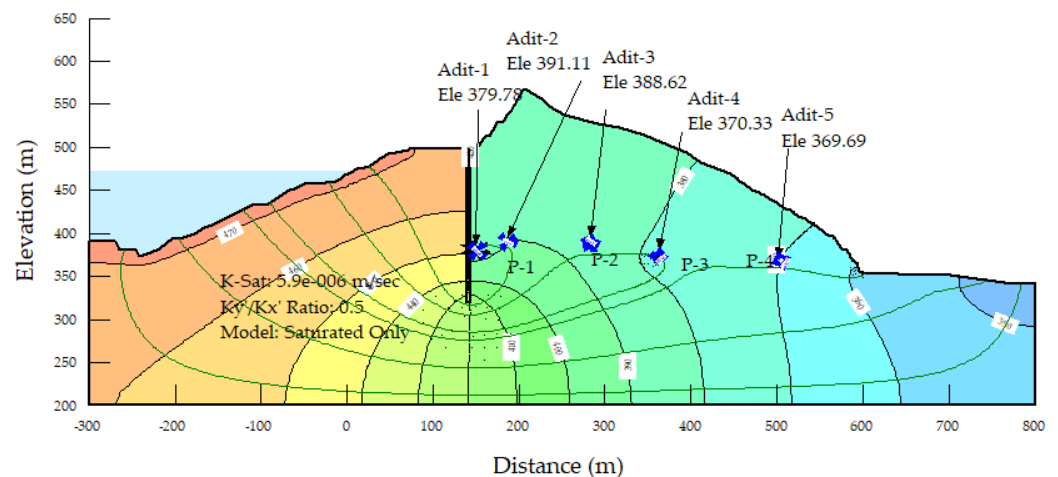
\* Visual observation.



**Figure 8.** Typical subsurface profile of rock mass at the study area.

**Table 5.** Summary of geotechnical and geological engineering parameters' typical range obtained in rock mass.

Sr. No.	Test Parameters	Igneous	Metamorphic	Sedimentary
1	Bulk Density (gm/cm <sup>3</sup> )	2.83–3.72	2.66–3.24	2.63–2.81
2	Natural Moisture Content (%)	0.08–0.40	0.15–3.34	0.22–0.97
3	Water Absorption (%)	0.06–0.60	0.52–1.19	0.29–1.45
4	Specific Gravity	2.86–3.78	2.69–3.30	2.71–2.85
5	Unconfined Compressive Strength (MPa)	14–274	14–153	43–105
6	Point Load Strength (MPa)	1.84–15.58	0.61–6.03	1.05–5.51
7	Brazilian Tensile Strength (MPa)	8.79–19.91	7.58–11.06	7.29–22.02
8	Hoek Direct Shear Test c (MPa)	0.01–0.53	-	7.29–13.56
9	Friction angle $\phi$ (deg)	21.1–42.1	-	14.29–13.56
10	Young's Modulus (MPa)	17,400–301,000	17,200–82,600	28,100–69,900
11	Poisson's Ratio	0.02–0.45	0.03–0.50	0.33–0.34
12	Hydraulic Conductivity (cm/sec)	$0.4 \times 10^{-4}$ – $8.5 \times 10^{-4}$	$0.8 \times 10^{-4}$	$0.2 \times 10^{-4}$ – $10 \times 10^{-4}$

**Figure 9.** Cross-section showing topography and location of instrumentation point.**Figure 10.** Results of seepage analysis.

The field database of seepage characteristics determined through adits and piezometers were used to validate the results of the Seep W model. A number of plots were developed comparing response of rock mass seepage against variation in rock mass hydraulic conductivity factors (Figures 11 and 12).

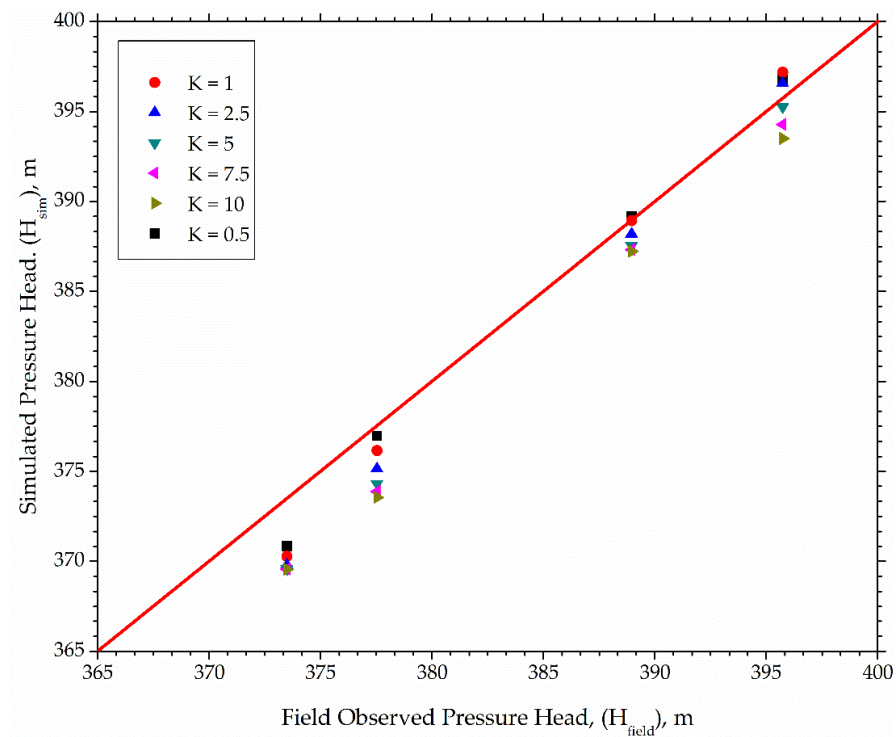


Figure 11. Pressure head observed vs. simulated pressure head from Seep W.

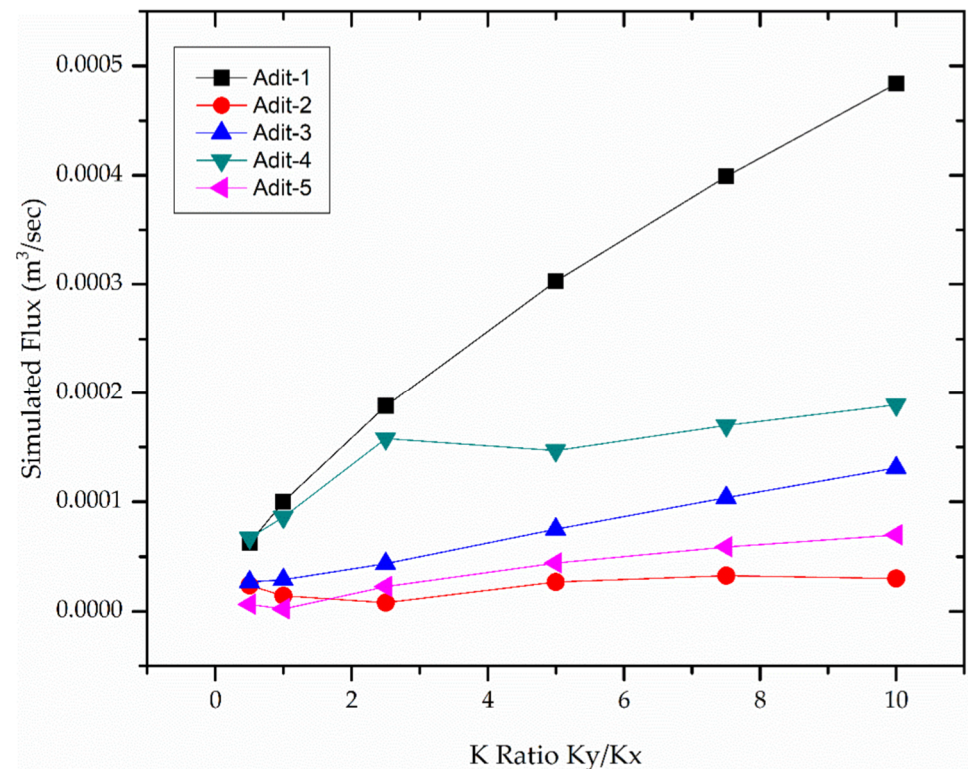


Figure 12. Trend between hydraulic conductivity K ratio ( $K_y/K_x$ ) vs. Seep W flux.

Figure 11 shows comparison results of field observed pressure head ( $H_{field}$ ) of four piezometers (P1–P4) and simulated pressure head ( $H_{sim}$ ) measured from the Seep W model. The typical range of  $H_{field}$  observed was from 373 to 397 and  $H_{sim}$  from 369 to 398, respectively. The pressure head values were plotted for K ratio ( $K_y/K_x$ ). A reference line of 45 degree was drawn to see the trend of values. The pressure head shows an

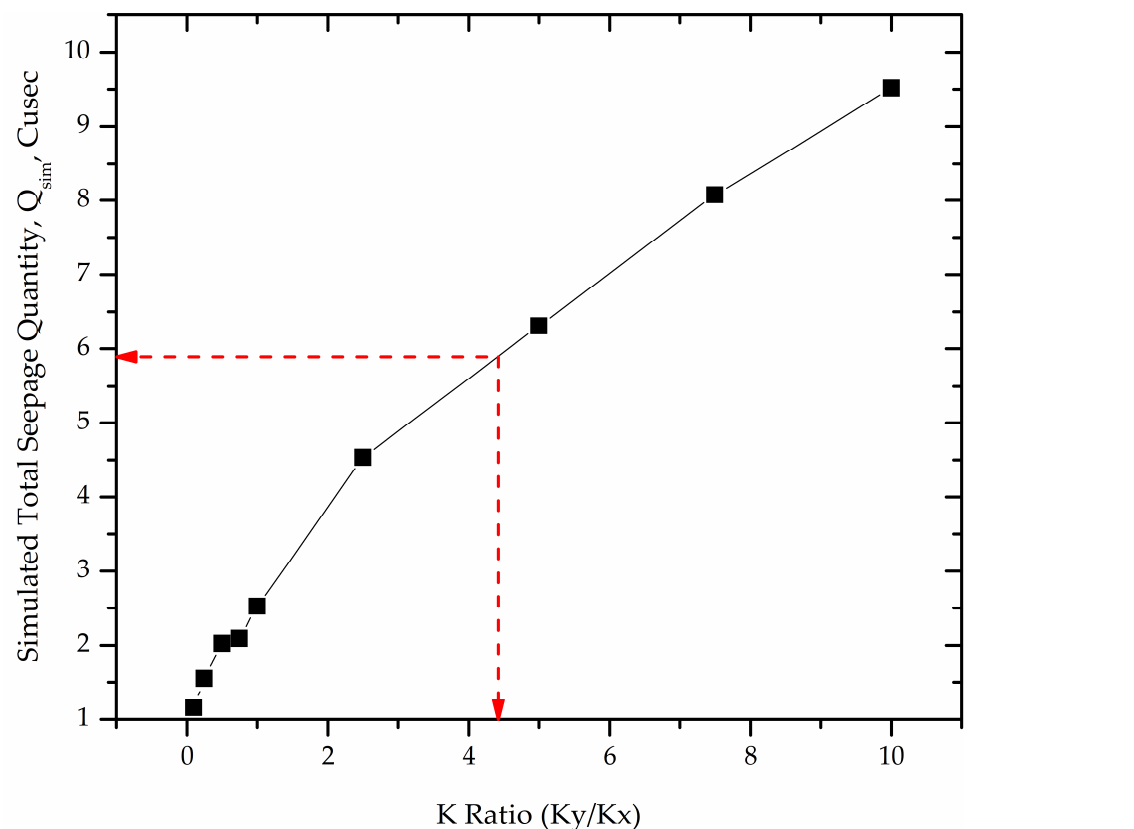
increasing trend with the increase in K Ratio ( $K_y/K_x$ ) from 0.5 to 10.  $H_{sim}$  and  $H_{field}$  show good agreement.

Figure 12 represents the results of the Seep W flux values at the location of five selected adits (adit 1–adit 5). The flux values were plotted for K ratio ( $K_y/K_x$ ). The flux values show overall an increasing trend in most of the data points with the increase in K Ratio ( $K_y/K_x$ ).

Seep W has the capability to evaluate the anisotropy coefficient termed K ratio, i.e., K ratio =  $K_y/K_x$ .  $K_x$  is always specified, and  $K_y$  is always computed from the specified K ratio.

$$K_y = \text{K ratio} \times K_x$$

It can be seen in Figure 13, that with increase in K ratio from 0.1 to 10, the seepage increases, which reflects that with increase in  $K_y$  and or  $K_x$  values the seepage also increases. Figure 10 also shows the trend of K ratio with the total simulated seepage quantity of the rock mass determined from Seep W. It was observed from the instrumentation data (seepage from adits) that the actual seepage quantity as accumulative value of all the five adits was 5.90 cusec. The same is marked in Figure 13. It was noticed that the K ratio against 5.90 cusec value was 4.43. The lower and upper range of K ratio was taken as 0.1 to 10 with reference to the K ratio value of 4.43. The corresponding  $K_y$  for a K ratio of 4.43 was  $2.6 \times 10^{-5}$  m/sec. The variation of seepage quantity with hydraulic conductivity anisotropy parameter K ratio from 0.1 to 10 reveals that the rock discontinuities aligned with the vertical axis can contribute to higher seepage quantity and uplift pressure as compared to lying parallel to the horizontal axis.



**Figure 13.** K ratio trend for seepage estimation.

A plot of all data points of hydraulic conductivity against respective RQD was prepared (Figure 14). The non-representative data points of wash out and failed Lugeon tests were omitted in the plots between RQD and hydraulic conductivity presented below. It was observed that at the junction of rock mass, the RQD values in the boreholes were relatively non-representative with depth. Further, during any abrupt variation in rock type,

the non-representative RQD values were observed. The hydraulic conductivity obtained against these non-representative values while potting was not giving the clear trend. A regression analysis was carried out between representative data points and a relationship was developed (Figure 14a) using best fitted logarithmic analysis, which is shown below.

$$Ka = 0.00129 - 2.90347 \times 10^{-4} \ln (RQD - 1.13595) (R^2 = 0.85) \quad (3)$$

where  $Ka$  is apparent hydraulic conductivity in cm/sec and RQD is in percentage.

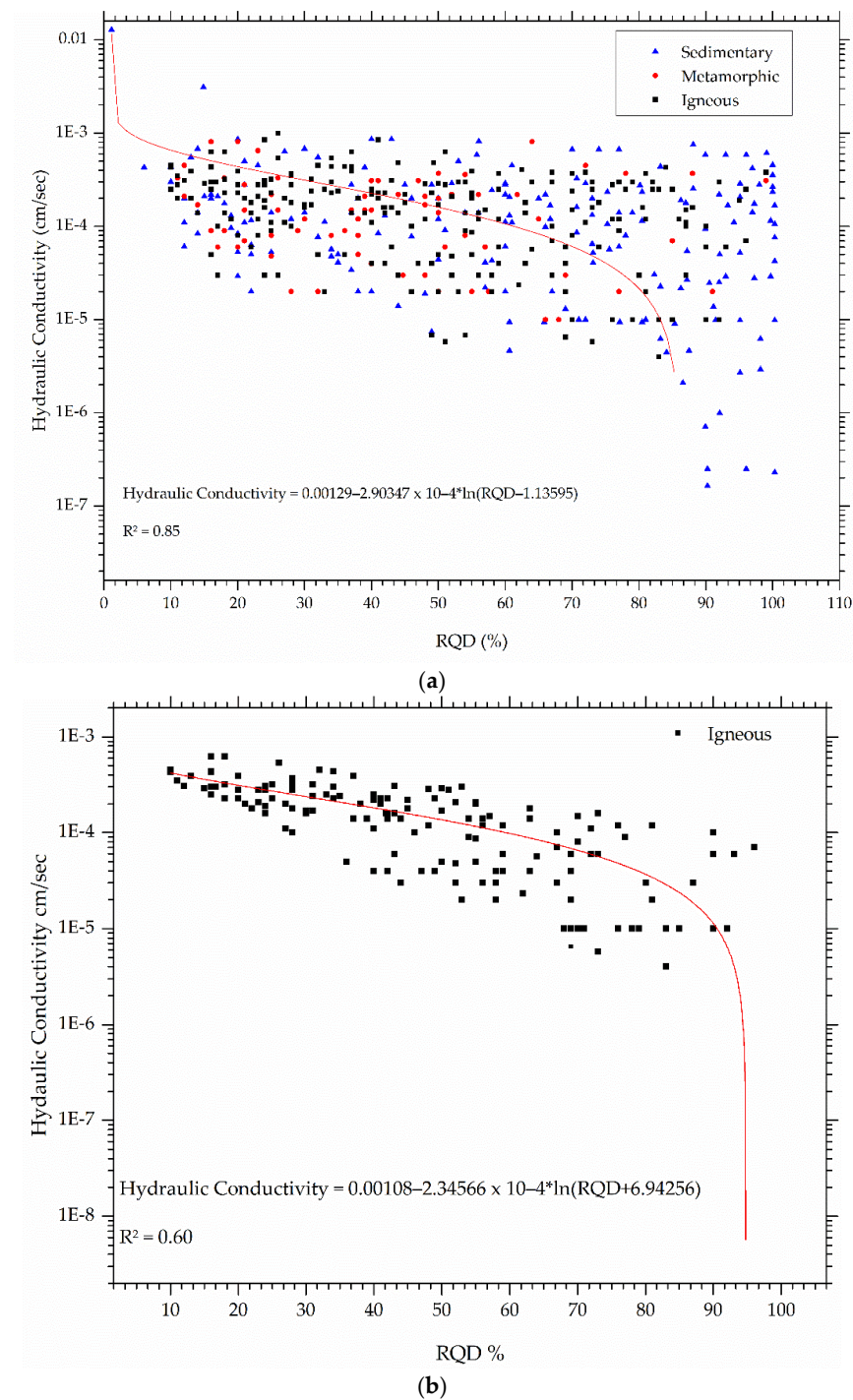
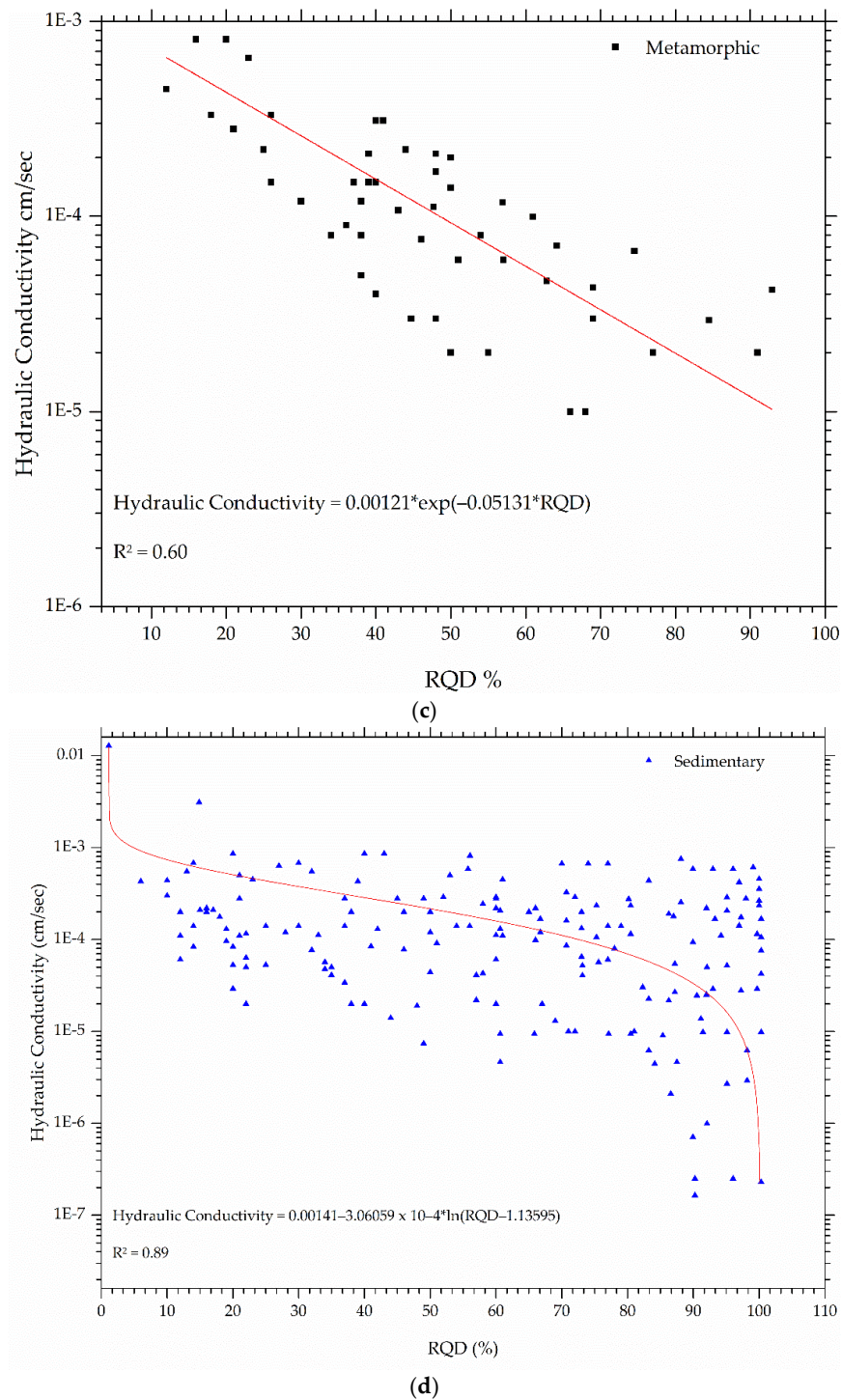


Figure 14. Cont.



**Figure 14.** Correlations between hydraulic conductivity and RQD; (a) rock mass, (b) igneous rock, (c) metamorphic rock, (d) sedimentary rock.

Three different plots were also prepared, which were extracted from the data of Figure 14. The values of hydraulic conductivity against RQD were analyzed using logarithmic regression model (three parameter logarithmic function) for igneous and sedimentary rock mass while exponential regression model (two parameter exponential function) for metamorphic rock mass. The best fit result is presented in Figure 14b for igneous, in Figure 14c for metamorphic, and in Figure 14d for sedimentary rock mass. The correlation was developed and provided below:

For igneous rocks:

$$Ka = 0.00108 - 2.34566 \times 10^{-4} \ln (RQD + 6.94256) (R^2 = 0.60) \quad (4)$$

For metamorphic rock:

$$Ka = 0.00121^{(-0.05131RQD)} (R^2 = 0.60) \quad (5)$$

For sedimentary rock:

$$Ka = 0.00141 - 3.06059 \times 10^{-4} \ln (RQD - 1.13595) (R^2 = 0.89) \quad (6)$$

While analyzing Figure 14, a strong correlation was observed between K and RQD for rock mass composite formation and sedimentary rock deposits. Reasonable correlation does exist between RQD and K for igneous and metamorphic rock deposits. These correlations can be used for evaluation of rock mass hydraulic conductivity using RQD data particularly during planning process of infrastructure development. These correlations proposed in this research can be used in relatively continuous rock mass formations. However, the applicability of these correlations in fractured rock mass needs to be further investigated. Sustainable infrastructure development requires realistic K determination, which is very often a costly and time-consuming undertaking. The determination of seepage characteristics of rock mass during preliminary design sometimes is also not affordable. These correlations help the engineers working in design to assess the rock mass seepage characteristics with confidence in similar rock mass formations.

#### 4. Conclusions

A detailed literature/reconnaissance survey was carried out in the Hazara formation to finalize rock mass formation. The geological and geotechnical engineering data were analyzed for the evaluation of the RQD and hydraulic conductivity of rock mass. The seepage response of the rock mass was determined from the geo-mechanical engineering data of the developed infrastructures. The seepage and pressure head data from the adits and installed piezometers were analyzed using the Finite Element Model (FEM) and results were compared with actual seepage observed in the rock mass from instrumentation. The following conclusions can be drawn from the above findings:

- A strong correlation exists between RQD and hydraulic conductivity of the composite rock mass formation.

$$Ka = 0.00129 - 2.90347 \times 10^{-4} \ln (RQD - 1.13595) (R^2 = 0.85)$$

- Reasonable correlations do exist between RQD and hydraulic conductivity of the individual rock types.

$$Ka = 0.00108 - 2.34566 \times 10^{-4} \ln (RQD + 6.94256) (R^2 = 0.60) \text{ (Igneous rocks)}$$

$$Ka = 0.00121^{(-0.05131RQD)} (R^2 = 0.60) \text{ (Metamorphic rock)}$$

$$Ka = 0.00141 - 3.06059 \times 10^{-4} \ln (RQD - 1.13595) (R^2 = 0.89) \text{ (Sedimentary rock)}$$

- The variation of seepage quantity with hydraulic conductivity anisotropy parameter K ratio reveals that the rock discontinuities contributing to a higher K ratio can contribute to higher seepage quantity and uplift pressure as compared to discontinuities resulting in a lower K ratio.

The instrumentation in the large infrastructures in such rock mass deposits is recommended from a sustainability perspective. These correlations help the engineers working in design to assess the rock mass seepage characteristics with confidence in similar rock mass formations.

**Author Contributions:** M.N.K.: conceptualization; data curation; formal analysis; methodology; writing—original draft. A.H.K.: supervision; resources; writing—review and editing. Z.u.R.: resources; writing—review and editing. T.S.C.: writing—review and editing. All authors have read and agreed to the published version of the manuscript.

**Funding:** This research received no external funding.

**Institutional Review Board Statement:** Not applicable.

**Informed Consent Statement:** Not applicable.

**Data Availability Statement:** Not applicable.

**Acknowledgments:** The authors are thankful to WAPDA for provision of data for present study and Tarbela 4th Consultants JV [43] for necessary coordination in this regard.

**Conflicts of Interest:** The authors declare no conflict of interest.

## References

- Jiang, T.; Shen, Z.; Liu, Y.; Hou, Y. Carbon Footprint Assessment of Four Normal Size Hydropower Stations in China. *Sustainability* **2018**, *10*, 2018. [[CrossRef](#)]
- Tang, W.; Li, Z.; Tu, Y. Sustainability Risk Evaluation for Large-Scale Hydropower Projects with Hybrid Uncertainty. *Sustainability* **2018**, *10*, 138. [[CrossRef](#)]
- Rasolofosaon, P.; Zinszner, B. Comparison between permeability anisotropy and elasticity anisotropy of reservoir rocks. *Geophysics* **2002**, *67*, 230. [[CrossRef](#)]
- Quinones-Rozo, C. Lugeon Test Interpretation, Revisited. In Proceedings of the 30th Annual USSD Conference, Sacramento, CA, USA, 12–16 April 2010; pp. 405–414.
- Öge, İ.F. Assessing Rock Mass Permeability Using Discontinuity Properties. *Procedia Eng.* **2017**, *191*, 638–645. [[CrossRef](#)]
- Al-Yaarubi, A.H.B. *Numerical and Experimental Study of Fluid Flow in a Rough-Walled Rock Fracture*; Imperial College: London, UK, 2003.
- Fan, Z.Q.; Jin, Z.-H.; Johnson, S.E. Modelling petroleum migration through microcrack propagation in transversely isotropic source rocks. *Geophys. J. Int.* **2012**, *190*, 179–187. [[CrossRef](#)]
- Fan, Z.; Eichhubl, P.; Newell, P. Basement Fault Reactivation by Fluid Injection into Sedimentary Reservoirs: Poroelastic Effects. *J. Geophys. Res. Solid Earth* **2019**, *124*, 7354–7369. [[CrossRef](#)]
- Gowida, A.; Moussa, T.; Elkatatny, S.; Ali, A. A Hybrid Artificial Intelligence Model to Predict the Elastic Behavior of Sandstone Rocks. *Sustainability* **2019**, *11*, 5283. [[CrossRef](#)]
- Zhang, C.; Li, D.; Wu, S.; Chen, L.; Peng, J. Study on Evolution Mechanism of Structure-Type Rockburst: Insights from Discrete Element Modeling. *Sustainability* **2021**, *13*, 8036. [[CrossRef](#)]
- El-Naqa, A. The hydraulic conductivity of the fractures intersecting Cambrian sandstone rock masses, central Jordan. *Environ. Geol.* **2001**, *40*, 973–982. [[CrossRef](#)]
- Qureshi, M.; Khan, K.; Bessaih, N.; Al-Mawali, K.; Al-Sadrani, K. An empirical relationship between in-situ permeability and RQD of discontinuous sedimentary rocks. *Electron. J. Geotech. Eng.* **2014**, *19*, 4781–4790.
- Ahmad, K.; Kristály, F.; Docs, R. Effects of clay mineral and physico-chemical variables on sandstone rock permeability. *J. Oil Gas Petrochem. Sci.* **2018**, *1*, 18–26. [[CrossRef](#)]
- Hamm, S.-Y.; Kim, M.; Cheong, J.-Y.; Kim, J.-Y.; Son, M.; Kim, T.-W. Relationship between hydraulic conductivity and fracture properties estimated from packer tests and borehole data in a fractured granite. *Eng. Geol.* **2007**, *92*, 73–87. [[CrossRef](#)]
- Lu, H.; Zhang, Y.; Zhang, G.; Zhang, M. A Thermal Effect Model for the Impact of Vertical Groundwater Migration on Temperature Distribution of Layered Rock Mass and Its Application. *Water* **2021**, *13*, 1285. [[CrossRef](#)]
- Priest, S.D. *Discontinuity Analysis for Rock Engineering*; Springer: Berlin/Heidelberg, Germany, 1993.
- Tsang, C.-F.; Neretnieks, I. Flow Channeling in Heterogeneous Fractured Rocks. *Rev. Geophys.* **1998**, *36*, 275–298. [[CrossRef](#)]
- Youn, D.; Gutierrez, M. Effect of Fracture Distribution on Permeability of Fractured Rock Masses. In Proceedings of the 45th U.S. Rock Mechanics/Geomechanics Symposium, San Francisco, CA, USA, 1 January 2011; p. 7.
- Zhang, Z. Hydro Mechanical Behaviour and Nonlinear Flow Characteristic of Rock Fractures. Ph.D. Thesis, University of Wollongong, Wollongong, Australia, 2013.
- Zhang, Z.; Nemcik, J. Fluid flow regimes and nonlinear flow characteristics in deformable rock fractures. *J. Hydrol.* **2013**, *477*, 139–151. [[CrossRef](#)]

21. Zhang, Z.; Nemcik, J. Friction Factor of Water Flow Through Rough Rock Fractures. *Rock Mech. Rock Eng.* **2013**, *46*, 1125–1134. [[CrossRef](#)]
22. Zhu, Z.; Niu, Z.; Que, X.; Liu, C.; He, Y.; Xie, X. Study on Permeability Characteristics of Rocks with Filling Fractures Under Coupled Stress and Seepage Fields. *Water* **2020**, *12*, 2782. [[CrossRef](#)]
23. Baghbanan, A.; Jing, L. Stress effects on permeability in a fractured rock mass with correlated fracture length and aperture. *Int. J. Rock Mech. Min. Sci.* **2008**, *45*, 1320–1334. [[CrossRef](#)]
24. Li, Z.; Liu, H.; Dun, Z.; Ren, L.; Fang, J. Grouting effect on rock fracture using shear and seepage assessment. *Constr. Build. Mater.* **2020**, *242*, 118131. [[CrossRef](#)]
25. Donnelly, C.R. Icold 2015-Question 97, Spillways-Évacuateurs de Crues. In Proceedings of the 25th International Congress on Large Dams, Stavanger, Norway, 7 July 2015.
26. Donnelly, C.R.; Acharya, A. A Discussion on the Evolution and Application of Quantitative Risk Informed Dam Safety Decision Making. In Proceedings of the 1st International Conference on Dam Safety Management and Engineering, Penang, Malaysia, 21 November 2019.
27. Moeini, H.; Farhadian, H.; Nikvar-Hassani, A. Determination of the optimum sealing method for Azad pumped storage dam considering seepage analysis. *Arab. J. Geosci.* **2018**, *11*, 389. [[CrossRef](#)]
28. Zhang, Q.-H.; Liu, Q.-B.; Su, A.-J.; Li, Y.-J.; Zhang, Y.-H. Hydraulic Conductivity of Rock Masses Surrounding Water Curtain Boreholes for Underground Oil Storage Caverns. *Energies* **2021**, *14*, 4588. [[CrossRef](#)]
29. Kassab, M.A.; Abuseda, H.H.; El Sayed, N.A.; LaLa, A.M.; Elnaggar, O.M. Petrographical and petrophysical integrated studies, Jurassic rock samples, North Sinai, Egypt. *Arab. J. Geosci.* **2016**, *9*, 99. [[CrossRef](#)]
30. Wang, J.C.; Wang, C.Y.; Tang, X.J.; Hu, S.; Han, Z.; Wang, Y.T. A method for estimating rock mass joint size using borehole camera technique. *Yantu Lixue/Rock Soil Mech.* **2017**, *38*, 2701–2707. [[CrossRef](#)]
31. Xue, Y.; Liu, Y.; Dang, F.; Liu, J.; Ma, Z.; Zhu, L.; Yang, H. Assessment of the Nonlinear Flow Characteristic of Water Inrush Based on the Brinkman and Forchheimer Seepage Model. *Water* **2019**, *11*, 855. [[CrossRef](#)]
32. Arshad, I.; Muhammad Munir, B. Comparison of SEEP/W Simulations with Field Observations for Seepage Analysis through an Earthen Dam (Case Study: Hub Dam-Pakistan) Comparison of SEEP/W Simulations with Field Observations for Seepage Analysis through an Earthen Dam (Case Study: Hub Dam-Pakistan). *Int. J. Res.* **2014**, *1*, 57–70.
33. Bear, J. *Dynamics of Fluids in Porous Media*; Courier Corporation: Chelmsford, MA, USA, 2013.
34. Chouireb, M.; Djehiche, A. Simulation of seepage flow through an earthen dam with vertical drain and comparison of results with observations data (case study: Harreza dam-Algeria). *Arab. J. Geosci.* **2019**, *12*, 406. [[CrossRef](#)]
35. Khaleel, R. Scale dependence of continuum models for fractured basalts. *Water Resour. Res.* **1989**, *25*, 1847–1855. [[CrossRef](#)]
36. Li, H.; Tian, H.; Ma, K. Seepage Characteristics and Its Control Mechanism of Rock Mass in High-Steep Slopes. *Processes* **2019**, *7*, 71. [[CrossRef](#)]
37. Long, J.C.S.; Remer, J.S.; Wilson, C.R.; Witherspoon, P.A. Porous media equivalents for networks of discontinuous fractures. *Water Resour. Res.* **1982**, *18*, 645–658. [[CrossRef](#)]
38. Min, K.-B.; Jing, L.; Stephansson, O. Determining the equivalent permeability tensor for fractured rock masses using a stochastic REV approach: Method and application to the field data from Sellafield, UK. *Hydrogeol. J.* **2004**, *12*, 497–510. [[CrossRef](#)]
39. Niu, Z.; Zhu, Z.; Que, X. Constitutive Model of Stress-Dependent Seepage in Columnar Jointed Rock Mass. *Symmetry* **2020**, *12*, 160. [[CrossRef](#)]
40. Turturro, A.C.; Caputo, M.C.; Perkins, K.S.; Nimmo, J.R. Does the Darcy–Buckingham Law Apply to Flow through Unsaturated Porous Rock? *Water* **2020**, *12*, 2668. [[CrossRef](#)]
41. Xia, C.; Lu, G.; Bai, D.; Zhu, Z.; Luo, S.; Zhang, G. Sensitivity Analyses of the Seepage and Stability of Layered Rock Slope Based on the Anisotropy of Hydraulic Conductivity: A Case Study in the Pulang Region of Southwestern China. *Water* **2020**, *12*, 2314. [[CrossRef](#)]
42. Karakuş, H.; Erguler, Z.A.; Ediz, İ.G.; Beyhan, S. Assessment of hydraulic conductivity of disturbed and undisturbed rock masses in Tunçbilek lignite basin, Turkey. *Arab. J. Geosci.* **2021**, *14*, 1522. [[CrossRef](#)]
43. WAPDA. *Design Report for Tarbela 4th Extension Hydropower Project*; WB-P115893; World Bank: Washington, DC, USA, 2012.
44. ASTM D2216; Standard Test Methods for Laboratory Determination of Water (Moisture) Content of Soil and Rock by Mass. ASTM International: West Conshohocken, PA, USA, 2019.
45. ASTM D6473; Standard Test Method for Specific Gravity and Absorption of Rock For Erosion Control. ASTM International: West Conshohocken, PA, USA, 2015.
46. ASTM D7012; Standard Test Methods for Compressive Strength and Elastic Moduli of Intact Rock Core Specimens under Varying States of Stress and Temperatures. ASTM International: West Conshohocken, PA, USA, 2014.
47. ASTM D5731; Standard Test Method for Determination of the Point Load Strength Index of Rock and Application to Rock Strength Classifications. ASTM International: West Conshohocken, PA, USA, 2016.
48. ASTM D3967; Standard Test Method for Splitting Tensile Strength of Intact Rock Core Specimens. ASTM International: West Conshohocken, PA, USA, 2016.
49. ASTM D5607; Standard Test Method for Performing Laboratory Direct Shear Strength Tests of Rock Specimens Under Constant Normal Force. ASTM International: West Conshohocken, PA, USA, 2016.